Raman Spectroscopy Study of α-, β-, γ-Na_xCoO_2 and γ-$(Ca,Sr)_xCoO_2$

H.X. Yang, Y. Xia, Y.G. Shi, H.F. Tian, R.J. Xiao, X. Liu, Y.L. Liu and J.Q. Li*

Beijing National Laboratory for Condensed Matter Physics, Institute of Physics, Chinese Academy of Sciences, Beijing 100080, China

Raman spectroscopy measurements have been performed on α-, β-, and γ-Na_xCoO_2 phases differing in their stacking of CoO_6 octahedra along the *c*-axis direction. The results demonstrate that, in general, there are five active phonons for γ-$Na_{0.75}CoO_2$, two Raman active phonons for α-$NaCoO_2$, and four Raman active phonons for β-$NaCoO_2$. We have also performed Raman scattering measurements on several γ-$(Ca,Sr)_xCoO_2$ ($0.15 \leq x \leq 0.35$) samples which show well-defined intercalated Ca/Sr-ordering. The experimental data show that the intercalated cation ordering could result in visible alterations on Raman spectral structures. The observations of the spectral changes along with the variation of the CoO_6 stacking, as well as the intercalated Sr/Ca ordering suggest that the interlayer interaction plays an important role for understanding the lattice dynamics in this layered system.

PACS numbers: 61.66. Fn, 78.30.–j, 68.65.Cd

Keywords: Na_xCoO_2; Cobalt oxides; Raman spectroscopy; Cation ordering

Author to whom correspondence should be addressed: Ljq@aphy.iphy.ac.cn

1. Introduction

Layered Na_xCoO_2 materials have been extensively investigated in recent years due to a notably large thermoelectric power coexisting with superconductivity and complex charge-ordering (CO) transitions [1-3]. In order to understand the lattice dynamics in this layered system, Raman scattering [4-9], infrared absorption [10], and neutron scattering experiments [11] have been carried out in numerous laboratories and under different experimental conditions. Theoretical analysis based on electronic band structures has also been performed for typical Na_xCoO_2 materials with x = 1.0, 0.5 and 0.3 [8, 12], however, much controversy still remains in related published results [4-12]. In our recent study, it is noted that the layered Na_xCoO_2 materials actually have a rich variety of structural features that could have visible effects on physical properties, such as, structural modulation from Na-ordering, phase transition with alternation of Na concentration, and essential sample (surface) instability with the ambient air and water. Hence, special precautions have to be taken for samples. There are three distinctive structural series of Na_xCoO_2 materials that differ in their stacking of CoO_6 octahedra along the *c*-axis direction, the so called α-, β-, and γ- phases respectively. The distance between two CoO_2 layers are almost the same for all three phases, each phase having its specific structural properties depend on Na concentration [13-19]. Cation ordering, commonly existing in layered Na_xCoO_2 materials, is another notable issue concerned in structural measurements and analysis of physical properties. For instance, certain experimental and theoretical investigations have paid special attention to intercalated Na ordering among CoO_2 sheets [6, 20], where the $3^{1/2}\times3^{1/2}$ superstructure was expected to have marked effects on the magnetic ordering in the layered

system [21]. Recently, we have synthesized a series of γ-Ca_xCoO_2 ($0.15 \leq x \leq 0.5$) and γ-Sr_xCoO_2 ($0.15 \leq x \leq 0.5$) by means of an ion exchange reaction. Structural analysis indicates that the average structures of these materials are isomorphic with the γ-Na_xCoO_2 phase. The well-defined cation ordering has been characterized by TEM observations [22, 23]. Moreover, M_xCoO_2 (M = Sr, Ca) compounds are found to be much more stable in the air than their analogous Na_xCoO_2 materials, thus $(Sr,Ca)_xCoO_2$ are more suitable for Raman observations [22, 23]. In the present paper, we will report on the Raman scattering measurements on the parent phases of α-, β-, γ-Na_xCoO_2 and on typical samples of γ-$(Sr,Ca)_xCoO_2$ ($0.15 \leq x \leq 0.35$). Certain spectral features have been also discussed in comparison with the theoretical analysis based on the group factor theory [24]

2. Experimental

Polycrystalline samples of α-$NaCoO_2$, β-$Na_{0.6}CoO_2$, γ-$Na_{0.75}CoO_2$ and $(Sr,Ca)_xCoO_2$ ($0.15 \leq x \leq 0.35$) materials were used in our Raman scattering study. The γ-$Na_{0.75}CoO_2$ phase was synthesized following the procedure as described in Ref [15], while α-$NaCoO_2$ and β-$Na_{0.6}CoO_2$ were prepared by conventional solid-state reactions at relatively lower temperatures of 500°C to 550°C [15]. In the synthesis of α-$NaCoO_2$ materials, powdered cobalt (Co) metal (99.5%) and 10% excess anhydrous NaOH pellets (Aldrich) (Na:Co = 1.1:1) were ground together under inert atmosphere and placed in an alumina boat under flowing O_2 for approximately 6 days at 500°C with one intermediate grinding. For the synthesis of β-$Na_{0.6}CoO_2$ material, the Co powder and NaOH pellets were mixed in a molar ratio of Na:Co = 0.7:1, ground together under flowing N_2, and then reacted under flowing O_2 at 550°C for approximately 5 days with one intermediate grinding. Polycrystalline

materials with nominal compositions of Sr_xCoO_2 and Ca_xCoO_2 ($0.15 \leq x \leq 0.35$) were prepared by a low-temperature ion exchange reaction using a γ-Na_xCoO_2 ($0.33 \leq x \leq 0.8$) precursor prepared by conventional solid-state reaction or by sodium deintercalation of $Na_{0.75}CoO_2$ [25]. The ion exchange process was carried out using the modified Cushing-Wiley method [26]. X-ray diffraction (XRD) measurements were carried out with a diffractometer in the Bragg-Brentano geometry using Cu K-α radiation. The compositions of all materials have been measured by an inductively coupled plasma (ICP) analysis technique. Raman spectra were collected using a back-scattering geometry at room temperature with a Jobin-Yvon T64000 triple spectrometer equipped with a cooled charge-couple device. In the spectrometer, an objective of 100X-magnification was used to focus the laser beam on the sample surface and collect the scattered light. Two excitation wavelengths at 488.0nm and 514.5 nm of an Ar^+ ion laser were used in our experiments. The laser power at the focus spot of 2-3 μm in diameter was kept below 1 mW to prevent laser-induced damage to the samples. For storage, the samples were rapidly put in a vacuum to avoid surface contamination and water adsorption. We did not choose low temperature storage, because the Na_xCoO_2 system has rich phase transitions with a lowering of the temperature and the cation order/disordering transition in this system is also very sensitive to temperature.

3. Results and discussion

Figure 1 shows the XRD patterns for the α-$NaCoO_2$, β-$Na_{0.6}CoO_2$ and γ-$Na_{0.75}CoO_2$ phases. These phases differ crystallographically in the stacking patterns of CoO_6 octahedra along the *c*-axis direction [13-19]. In the α-Na_xCoO_2 system, the parent phase with a

nominal composition of α-$NaCoO_2$ has a hexagonal cell with lattice parameters of a = 2.89 Å, c = 15.59 Å ($R\bar{3}$m space group) [18]; the parent sample β-$Na_{0.6}CoO_2$ has a monoclinic structure with a C2/m space group and lattice parameters a = 4.90 Å, b =2.83 Å, c = 5.71 Å, β = 106.180° [19]; The parent material of γ-$Na_{0.75}CoO_2$ has a hexagonal cell with lattice parameters a = 2.84Å and c = 10.80Å ($P6_3/mmc$ space group) [11]. In recent studies, the γ-Na_xCoO_2 ($0.15 < x < 0.75$) materials were found to show a rich variety of significant physical properties [1-3], such as, a notably large thermoelectric power, superconductivity under water intercalation, and CO transitions for x~0.5.

Figure 1(b) shows the layered structural features of α-$NaCoO_2$, β-$Na_{0.6}CoO_2$ and γ-Na_xCoO_2. The α-$NaCoO_2$ contains three CoO_2 layers in one unit cell in which Na occupies the unique 3a (0,0,0) site, Co occupies the 3b (0,0,1/2) site, and O occupies the 6c (0,0,z) site [18]. The β-Na_xCoO_2 has a C2/m symmetry, its unit cell contains only one CoO_2 layer, Na occupies the 2a (0,0,0) site, Co occupies the 4i (x,0,z) site, and O occupies the 8j (x,y,z) site [19]. The γ-$Na_{0.75}CoO_2$ material contains two CoO_2 layers in one unit cell in which Co occupies the 2a (0,0,0) and O occupies the 4f (1/3,2/3,z) site, while the Na atoms in this structure could occupy two distinct sites within a given plane denoted with Wyckoff indices of 2b(Na_1) and 2d(Na_2) [11]. The occupation ratio on either Na_1 or Na_2 site depends on the Na content.

Based on this structural information, we have made a brief theoretical factor-group analysis for the Raman active modes in the α-, β- and γ-Na_xCoO_2 phases, based on the method as reported in Ref [24]. It is demonstrated that there are two Raman active phonon modes $A_{1g}+E_g$ for the α-$NaCoO_2$ phase, both connected with O motions; there are nine

active phonon modes: $5A_{1g}+4B_{1g}$ for β-$Na_{0.6}CoO_2$, three A_{1g} and three B_{1g} modes involve motions of the Na atoms only, and two A_{1g} and one B_{1g} mode involve motions of the oxygen atoms only. The γ-Na_xCoO_2 phase has five Raman active phonon modes: $A_{1g} + E_{1g} + 3E_{2g}$, the A_{1g} and E_{1g} modes involve motions of the oxygen atoms only, E_{2g} modes may connect with both Na and O motions while Co motions are not Raman active as discussed previously [4].

Fig. 2 shows the experimental Raman spectra for three typical phases. According to the conductivity measurements for these phases, the α-$NaCoO_2$ phase is a semiconductor at room temperature while β-$Na_{0.6}CoO_2$ and γ-Na_xCoO_2 phases are metallic [27]. An increase in conductivity reduces the optical skin depth of the incident laser beam, and results in a decrease in Raman scattering intensity. Hence, under the same experimental conditions the α-$NaCoO_2$ has a relatively higher signal/noise ratio. The experimental spectrum of α-$NaCoO_2$ contains two clear peaks found at 486.5 and 586.4cm^{-1}, respectively. We interpret theses peaks as the E_{1g} and A_{1g} active modes in agreement with above theoretical analysis [8]. The A_{1g} and E_{1g} modes involve atomic motions from oxygen atoms only: the E_{1g} represents the vibration along the in-plane diagonal directions, and the A_{1g} represents the out-of-plane movement. The energy of the A_{1g} mode strongly depends on the occupancy of the Na layer which divides the CoO_6 octahedral in the c-axis direction. It is worth mentioning that our experimental spectra for the α-Na_xCoO_2 phase shows noticeable similarities with results reported in Ref [5] and [9] obtained from Na_xCoO_2 single crystals. Hence, it is possible that the above referenced crystals (or crystal surfaces) crystallize in an α-phase structure rather than a γ-phase structure. Experimental spectra of β-$Na_{0.6}CoO_2$ in

general contain three or four visible peaks at around 461, 480, 577, and 691 cm^{-1}, as shown in Fig. 2. On the other hand, our theoretical factor-group analysis suggests that nine active modes ($5A_{1g}$+$4B_{1g}$) are possibly visible; this discrepancy could be caused by the overlap of Raman peaks. There are five Raman active modes that can be identified: A_{1g} at 673.3cm^{-1}, E_{1g} at 188.5cm^{-1}, and E_{2g} at 470.4cm^{-1}, 510.7cm^{-1}, and 605.8 cm^{-1} for γ-$Na_{0.75}CoO_2$, which agree well with our former detailed analysis on single crystals [4].

It is noted that the intercalations of Na, Sr, and Ca atoms or H_2O molecules could make the local structure of this layered system much more complex. The intercalated atoms can be random with high mobility or crystallized in a variety of ordered states [6, 20]. Certain ordered states were demonstrated to have notable effects on physical properties. For instance, Na atoms in $Na_{0.5}CoO_2$ crystallize in an orderly, well-defined zigzag pattern yielding an orthorhombic structure in which low temperature charge ordering is observed [6]. The Raman spectroscopy is sensitive to the ordered structures, and can be used effectively to characterize the degree and type of cation order in perovskite oxides [28]. Recently, experimental and theoretical investigations have paid special attention to intercalated cation/vacancy ordering in the layered cobalt oxides [6, 20]. First principle calculations demonstrated that a variety of possible ordered states can be stable at different levels of intercalated cation content, such as $3^{1/2}a\times3^{1/2}a$ superstructure at x = 1/3 (or 2/3) and other ordered states at x = 1/2, 1/4, 1/5, etc. [20]. Previously, several superstructures in Li_xCoO_2 and Na_xCoO_2 materials have been demonstrated to have cation ordering [6, 29]. However, it is also noted that the electron beam radiation during TEM observation could severely alter the cation arrangements among the CO_2 sheets due to the high mobility of

either Na or Li ions in this layered structure [6, 29].

In the present study, we have performed Raman scattering measurements on several γ-$(Ca,Sr)_xCoO_2$ ($0.15 \leq x \leq 0.35$) materials in which the cation ordered states were well demonstrated by means of selected-area electron diffraction and high-resolution TEM observations. Figs. 3(a) and (b) show respectively the electron-diffraction patterns and high-resolution TEM images for the $Sr_{0.35}CoO_2$. The most notable structural phenomenon revealed in the electron diffraction pattern of Fig. 3(a) is the appearance of systematic weak reflection spots in addition to the main diffraction spots indexed perfectly on the known hexagonal structure. The superstructure spots in the present case can be well characterized by an in-plane wave vector **q** = (1/3, 1/3, 0) which yields a $3^{1/2}a \times 3^{1/2}a$ super-cell within the basic *a*-*b* plane. The superlattice spots on the **a***-**b*** plane in general are very sharp, indicating a relatively long coherent length (>30nm) of the ordered state. Fig. 3(b) shows a [001] zone-axis HRTEM image for $Sr_{0.35}CoO_2$, illustrating the atomic structure for this superstructure. The image was obtained from a thin region of the crystal near the Scherzer defocus value (≈-60nm). The metal atom (Co) positions are therefore recognizable as dark dots. In this image, the hexagonal superstructure is clearly seen in the relative thick area as illustrated by a hexagonal supercell.

Raman scattering measurements on γ-Sr_xCoO_2 ($0.15 \leq x \leq 0.40$) materials have revealed notable changes of the Raman spectrum along with the appearance of cation ordered states. Fig. 4(a) shows a series of Raman spectra taken from the γ-Sr_xCoO_2 materials with x = 0.15, 0.25, and 0.35. It is noted that the Raman active modes for x = 0.15 and 0.25 show five clear active modes (with limited shifts) notably similar with the data

from γ-$Na_{0.75}CoO_2$ as shown in Fig.2. Actually, the intercalated Sr atoms in γ-Sr_xCoO_2 samples with $x < 0.25$ are rather random as observed for Na atoms in γ-$Na_{0.75}CoO_2$. Certain notable spectral features were observed in the data obtained from $Sr_{0.35}CoO_2$ which contains a well defined $3^{1/2}a \times 3^{1/2}a$ superstructure, in addition to the remarkable shift of the five typical peaks for the γ-$Sr_{0.15}CoO_2$ phase. New modes at ~148 cm^{-1} are also clearly visible.

In order to further understand the effects of intercalated cation ordering in the Raman spectra of this layered system, we have also performed measurements on the γ-Ca_xCoO_2 materials. This system, being similar to Sr_xCoO_2 and Na_xCoO_2, contains a rich variety of structural phenomena, such as Ca ordering and phase separation [23]. Fig. 4(b) displays the Raman spectra from the γ-Ca_xCoO_2 ($0.15 \leq x \leq 0.35$) materials. It is clearly recognized that the Raman peak intensities and frequencies vary visibly with the increase of Ca content. These facts, in combination with results from Sr_xCoO_2 and Na_xCoO_2, suggest that the lattice dynamics are somewhat sensitive to the variation of the cation ordering in the present system. The γ-$Ca_{0.15}CoO_2$ material has five active modes identified respectively as A_{1g} at 691.1cm^{-1}, E_{1g} at 196.6cm^{-1}, and E_{2g} at 483.3cm^{-1}, 525.1cm^{-1}, and 625.8 cm^{-1} that are comparable with the active modes of γ-$Sr_{0.15}CoO_2$ as discussed above. Moreover, it is remarkable that all the Raman active modes show significant shifts towards higher frequencies in comparison with those in the γ-$Na_{0.75}CoO_2$ sample, especially A_{1g} and E_{1g} peaks which are essentially connected with the O vibrations. This could be due to the larger electrostatic interaction between divalent ions and the negative CoO_2 layer in γ-$(Ca,Sr)_xCoO_2$ compounds.

Systematic structural analysis on γ-Ca_xCoO_2 suggests that there are two well-defined cation ordered states corresponding respectively to the orthorhombic superstructure at around x = 1/2 and the $3^{1/2}a\times3^{1/2}a$ superstructure at around x = 1/3 in this kind of system. Multiple ordered states, phase separation, and incommensurate structural modulations commonly appear in materials with 0.33 < x < 0.5. The Raman spectra from γ-$Ca_{0.3}CoO_2$ (see Fig.5) show the alternation of spectral features corresponding to a $3^{1/2}\times3^{1/2}$ superstructure. Further analysis shows that the A_{1g} mode at 691cm^{-1} shifts slightly to a higher frequency and the E_{2g} mode at 483 cm^{-1} shifts to a lower frequency in comparison with those for the x = 0.15 sample. Moreover, the two modes that appear at 560 and 595 cm^{-1} are possibly the remaining E_{2g} modes under significant shift, or new modes arising from local structural ordered states in the superstructure phase. The spectra of $Ca_{0.35}CoO_2$ and $Ca_{0.4}CoO_2$ shows certain combined features of $Ca_{0.15}CoO_2$ and $Ca_{0.30}CoO_2$, indicating the presence of local structural inhomogeneities in the samples studied, which agrees well with the structural analysis.

It is notable that the Raman scattering measurements on Na_xCoO_2 materials (polycrystalline samples or single crystals) performed in several laboratories show apparently different spectral features. For instance, P. Lemmens *et al*, reported Raman spectroscopy measurements on Na_xCoO_2 single crystals, with x = 0.5, 0.83, and 1.0. All spectra show two strong phonon modes at around 580 cm^{-1} and 480 cm^{-1}. These results are very similar with our data obtained from the α-$NaCoO_2$ phase. Experimental investigations should take special precautions when measuring single crystals obtained after post-chemical treatments, because these treatments, such as Na-deintercalation and H_2O

intercalation, may cause complex defects. We have carefully checked the microstructure of the single crystalline samples of $Na_{0.5}CoO_2$ and $Na_{0.3}CoO_2$ prepared by Na-deintercalation and it was observed that stacking faults and intergrowth of different phases occasionally appear in the samples. Fig. 5 shows the [010] zone-axis HRTEM image and the selected-area electron diffraction pattern taken from a $Na_{0.5}CoO_2$ single crystal prepared using Na-deintercalation. The coexistence of γ- and β- phases are clearly seen. The reflections in the diffraction pattern exhibit weak diffuse spots streaking along the c*- axis direction, indicating the presence of stacking faults and other planar defects in this system. It is interesting to point out that certain reported Raman scattering results for Na_xCoO_2, such as the spectra in Ref [5], can be interpreted by a combination of α, β, and γ phases in the range of 400 to 800 cm^{-1} [5].

4. Conclusions

The Raman scattering spectra obtained from the α, β, γ -Na_xCoO_2 phases, γ-Ca_xCoO_2 and γ-Sr_xCoO_2 ($0.15 \leq x \leq 0.35$) materials have been analyzed. In general, it is observed that five Raman active phonons around 186 cm^{-1} (E_{1g}), 470 cm^{-1}, 511 cm^{-1}, 606 cm^{-1} ($3E_{2g}$), 673 cm^{-1} (A_{1g}) appear in γ-$Na_{0.75}CoO_2$. Two Raman active phonons at 487 cm^{-1} (E_{1g}) and 587 cm^{-1} (A_{1g}) appear in α-Na_xCoO_2. The Raman active phonons in γ-$(Sr,Ca)_xCoO_2$ materials change systematically along with the intercalated cation ordering. These observations suggest that the interlayer interaction play an important role for understanding the lattice dynamics in this layered system. It is also worthy to point out that due to the complex defect structures and various ordering states in these kinds of materials, special precautions have to be taken for processing and interpreting the experimental data.

Acknowledgments

We would like to thank Professor N.L. Wang for providing single crystals of Na_xCoO_2 and Miss G. Zhu for assistance in preparing samples and measuring Raman spectra. We are grateful to N. Pemberton-Pigott for fruitful discussions and help during manuscript preparation. The work reported here is supported by the 'Outstanding Youth Fund' supported by the National Natural Foundation of China and by the Ministry of Science and Technology of China (973 project No: 2006CB601001).

References:

1. I. Terasaki, Y. Sasago, K. Uchinokura, *Phys. Rev. B,* **56**, R12685 (1997).
2. K. Takada, H. Sakurai, E. Takayama-Muromachi, F. Izumi, R.A. Dilanian and T. Sasaki, *Nature*, **422**, 53 (2003).
3. M.L. Foo, Y.Y. Wang, S. Watauchi, H.W. Zandbergen, T. He, R.J. Cava, and N.P. Ong, *Phys. Rev. Lett*. **92,** 247001 (2004).
4. Y.G. Shi, Y.L. Liu, H.X. Yang, C.J. Nie, R. Jin, J.Q. Li, *Phys. Rev. B*, **70,** 052502 (2004).
5. P. Lemmens, V. Gnezdilov, N.N. Kovaleva, *et al*., *J. Phy. : -Cond. Matt.,* **16**, S857-S865 (2004).
6. H.X. Yang, C.J. Nie, Y.G. Shi, H.C. Yu, S. Ding, Y.L. Liu, D. Wu, N.L. Wang, J.Q. Li, *Solid State Commun.***134,** 403 (2005).
7. X.N. Zhang, P. Lemmens, , V. Gnezdilov, K.Y. Choi, B. Keimer, D.P. Chen, C.T. Lin, F.C. Chou, *Physica B* **359-361,** 424 (2005).
8. M.N. Iliev, A.P. Litvinchuk, R.L. Meng, Y.Y. Sun, J. Cmaidalka, C.W. Chu. *Physica C,* **402,** 239 (2004).
9. P. Lemmens, K.Y. Choi, V. Gnezdilov, E.Ya.Sherman, D.P. Chen, C.T. Lin, F.C. Chou, B. Keimer, cond-mat/0510756.
10. N.L. Wang, D. Wu, G. Li, X.H. Chen, C.H. Wang, X.G. Lou, *Phys. Rev. Lett*. **93,** 147403 (2004)
11. J.W. Lynn, Q. Huang, C.M. Brown, V.L. Miller, M.L. Foo, R.E. Schaak, C. Y. Jones, E.A. Mackey, and R.J. Cava, *Phys. Rev. B* **68**, 214516 (2003).

12. Z.Y. Li, J.L. Yang, J.G. Hou and Q.S. Zhu, *Phys. Rev. B* **70**, 144518 (2004)

13. K. Takada, H. Sakurai, E. Takayama-Muromachi, F. Izumi, R.A. Dilanian, and T. Sasaki, *Adv. Mater.* **16**, 1901 (2004).

14. S. Mistry, D.C. Arnold, C. J. Nuttall, A. Lappas and M. A. Green, *Chem. Commun.*, 2440 (2004).

15. C. Fouassier, Gn. Matejka, J.-M. Reau, and P.J. Hagenmuller, *J. Solid State Chem*. **6**, 532 (1973).

16. T. Motohashi, R. Ueda, E. Naujalis, T. Tojo, I. Terasaki, T. Atake, M. Karppinen, H. Yamauchi, *Physical Review B* **67**,064406(2003).

17. M.L. Foo, T. Klimczuk, L Li, N.P. Ong, R.J. Cava. *Solid State Commun.* **133**, 407 (2005).

18. Y. Takahash, Y. Gotoh, J. Akimoto, *J. Solid State Chem*. **172**, 22 (2003).

19. Y. Ono, R. Ishikawa, Y. Miyazaki, Y. Ishii, Y. Morii, and T. Kajitani, *J. Solid State Chem.*, **166**, 177 (2002).

20. P.H. Zhang, R.B. Capaz, M.L. Cohen, S.G. Louie, *Phys. Rev. B*, **71**, 153102 (2005).

21. A. Van der Ven, M. K. Aydinol, G. Ceder, G. Kresse and J. Hafner, *Phys. Rev. B* **58**, 2975 (2004)

22. H.X. Yang, Y.G. Shi, X. Liu, R.J. Xiao, H.F. Tian and J.Q. Li, , *Phys. Rev. B* **73**, 014109 (2006).

23. H.X. Yang, Y.G. Shi, Y.Q. Guo, X. Liu, R.J. Xiao, J.L. Luo, J.Q. Li, *cond-mat/0503136.*

24. E. Kroumova, M.I. Aroyo, J.M. Perez-Mato, A. Kirov, C. Capillas, S. Ivantchev, H.

Wondratschek, *Phase Transitions* **76**, 155 (2003).

25. M. L. Foo, Y. Wang, S.Watauchi, H.W. Zandbergen, T. He, R.J. Cava, and N.P. Ong, *Phys. Rev. Lett.* **92**, 247001 (2004).
26. B.L. Cushing, J.B. Wiley, *J. Solid. State. Chem.* **141**, 385 (1998).
27. Y.G. Shi, H.X. Yang, H. Huang, X. Liu, and J.Q. Li, *Phys. Rev. B*, in press
28. I. Levin, S.A. Prosandeev, and J.E. Maslar, *Applied Physics Letters* 86, 011919 (2005).
29. H.W. Zandbergen, M. Foo, Q. Xu, V. Kumar, R.J. Cava, *Phys. Rev. B*, **70,** 024101 (2004).

Figure Captions

Fig. 1: (a) XRD patterns for parent phases of α-$NaCoO_2$, β-$Na_{0.6}CoO_2$ and γ-$Na_{0.75}CoO_2$. The lattice parameters for all phases are shown for comparison.

(b) Structural models of α-$NaCoO_2$, β-$Na_{0.6}CoO_2$ and γ-$Na_{0.75}CoO_2$ phases.

Fig. 2: Raman spectra of the α-$NaCoO_2$, β-$Na_{0.6}CoO_2$ and γ-$Na_{0.75}CoO_2$ phases, demonstrating different spectral structures for these specific phases.

Fig. 3: (a) Electron diffraction patterns and (b) HRTEM image taken along the [001] zone axis direction of $Sr_{0.35}CoO_2$, showing the $3^{1/2}\boldsymbol{a}\times3^{1/2}\boldsymbol{a}$ superstructure from Sr ordering.

Fig. 4: (a) Raman spectra taken from γ-Sr_xCoO_2 materials with x = 0.15, 0.25, and 0.35, showing the evident change of the spectral structures due to the $3^{1/2}\times3^{1/2}$ superstructure.

(b) Raman spectra taken from γ- Ca_xCoO_2 materials with x = 0.15, 0.3, 0.35, showing the spectral features arising from cation ordering.

Fig. 5: HRTEM and corresponding electron diffraction pattern taken alone [010] zone-axis, indicating the coexistence of different phases observed in the $Na_{0.5}CoO_2$ single crystals. The top region is governed mainly by the γ-phase and the bottom area is almost entirely β-phase.

Figure 1

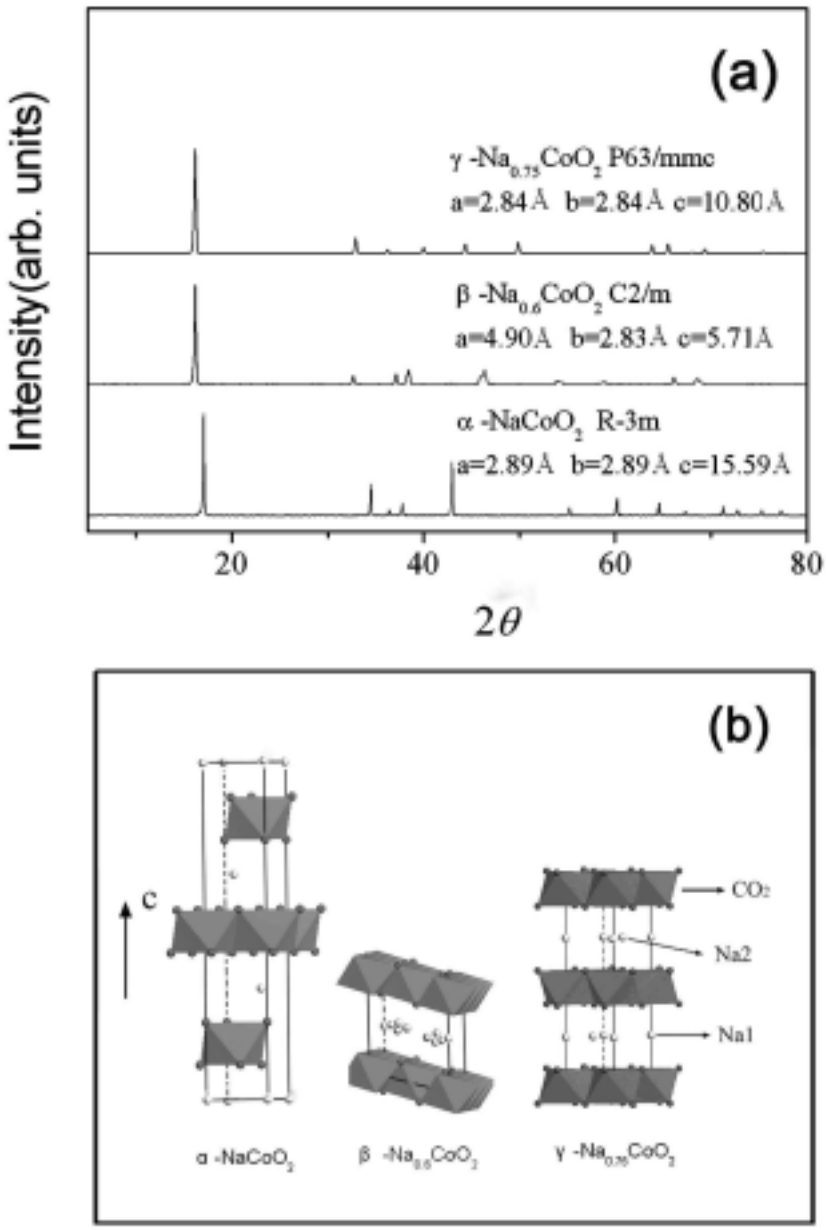
(a)
γ -Na0.75CoO2 P63/mmc
a=2.84Å b=2.84Å c=10.80Å
β -Na0.6CoO2 C2/m
a=4.90Å b=2.83Å c=5.71Å
α -NaCoO2 R-3m
a=2.89Å b=2.89Å c=15.59Å
Intensity(arb. units)
20
40
60
80
2θ
(b)
c
CO2
Na2
Na1
α -NaCoO2
β -Na0.6CoO2
γ -Na0.70CoO2

Figure 2

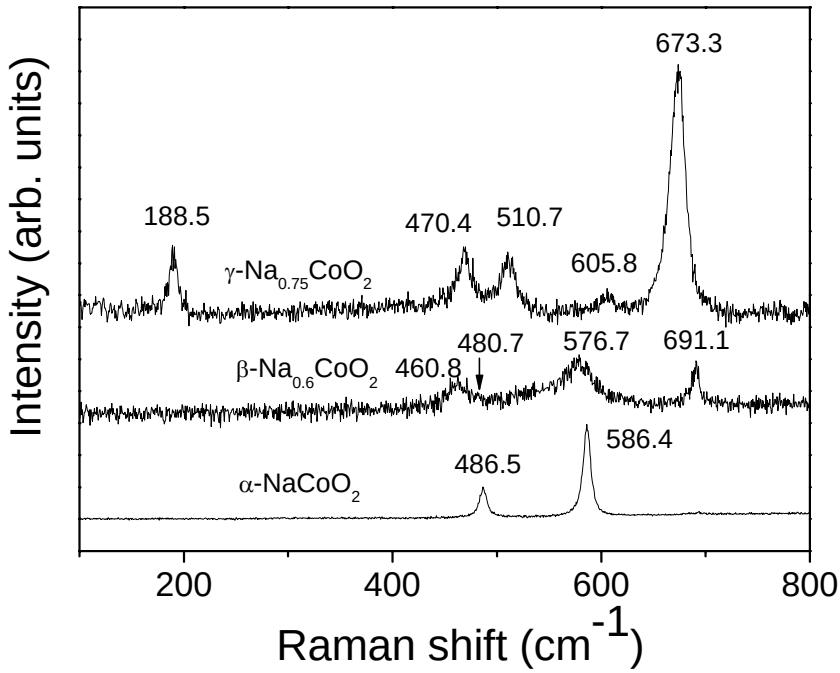
673.3
188.5
470.4
510.7
605.8
γ-Na0.75CoO2
480.7
576.7
691.1
β-Na0.6CoO2
460.8
586.4
486.5
α-NaCoO2
200
400
600
800
Intensity (arb. units)
Raman shift (cm-1)

Figure 3

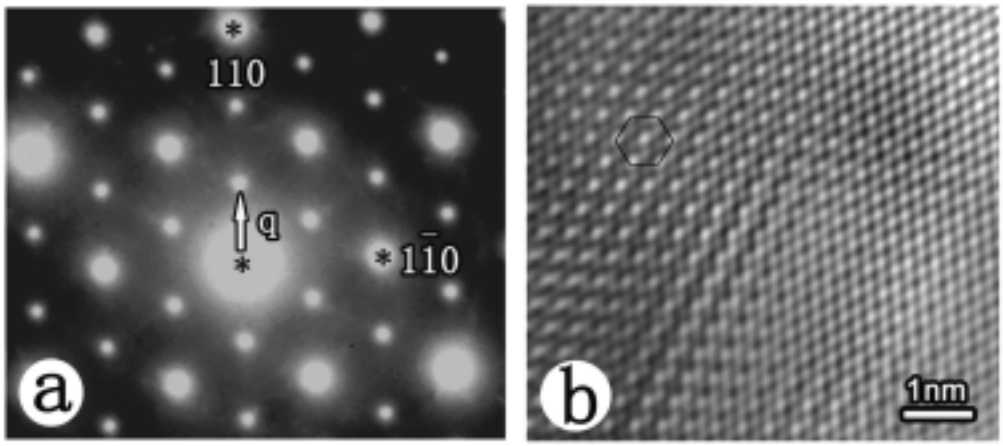

Figure 4

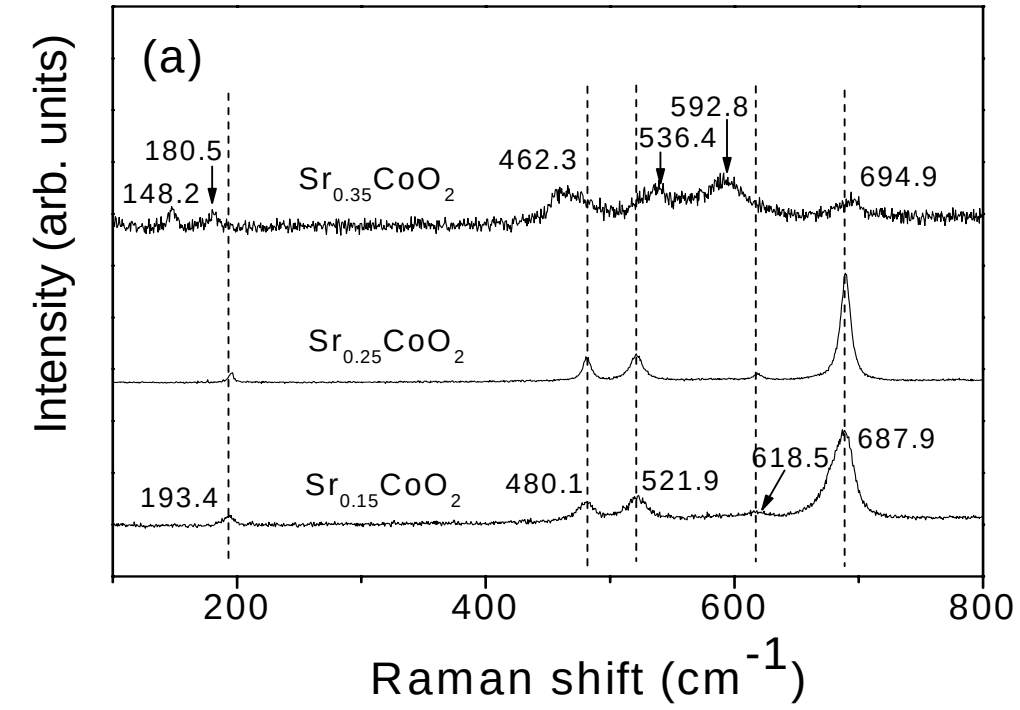
(a)
Intensity (arb. units)
180.5
148.2
Sr0.35CoO2
462.3
592.8
536.4
694.9
Sr0.25CoO2
193.4
Sr0.15CoO2
480.1
521.9
618.5
687.9
200
400
600
800
Raman shift (cm-1)

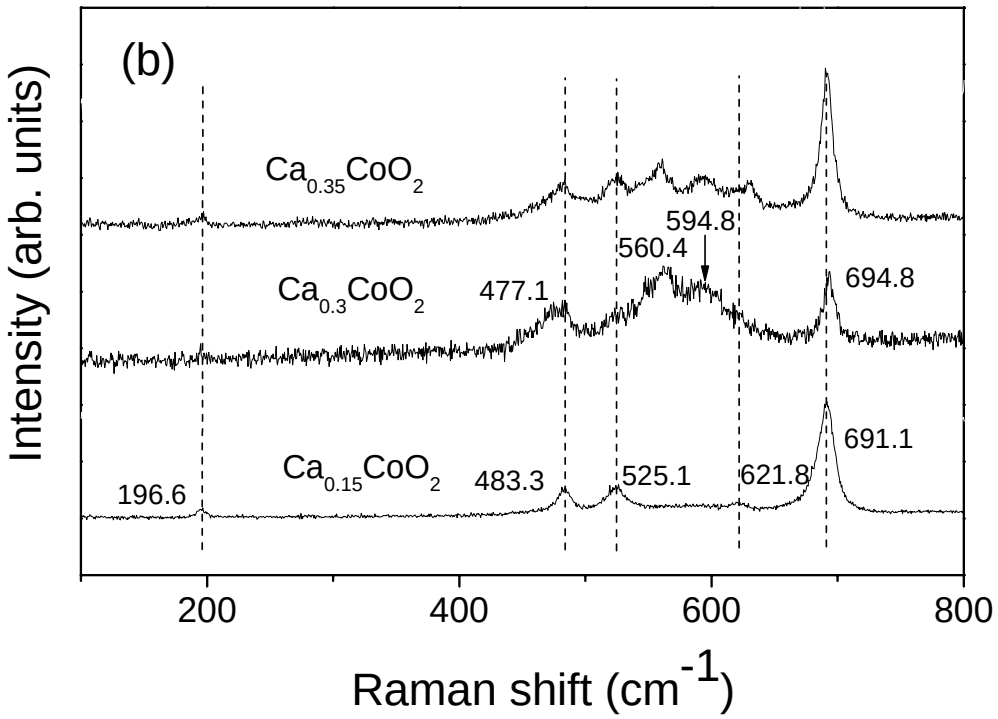
(b)
Intensity (arb. units)
Ca0.35CoO2
594.8
560.4
Ca0.3CoO2
477.1
694.8
691.1
Ca0.15CoO2
196.6
483.3
525.1
621.8
200
400
600
800
Raman shift (cm-1)

..

Figure 5